International Journal of Heat and Mass Transfer 136 (2019) 288–297

Contents lists available at ScienceDirect

International Journal of Heat and Mass Transfer

journal homepage: www.elsevier.com/locate/ijhmt

Unsteady flow and heat transfer past a stretching/shrinking sheet in a hybrid nanofluid

Iskandar Waini [a], Anuar Ishak [b], Ioan Pop [c,*]

[a] Fakulti Teknologi Kejuruteraan Mekanikal dan Pembuatan, Universiti Teknikal Malaysia Melaka, Hang Tuah Jaya, 76100 Durian Tunggal, Melaka, Malaysia
[b] School of Mathematical Sciences, Faculty of Science and Technology, Universiti Kebangsaan Malaysia, 43600 UKM Bangi, Selangor, Malaysia
[c] Department of Mathematics, Babeş-Bolyai University, 400084 Cluj-Napoca, Romania

ARTICLE INFO

Article history:
Received 27 November 2018
Received in revised form 30 January 2019
Accepted 28 February 2019

Keywords:
Unsteady
Hybrid nanofluids
Stretching/shrinking sheet
Dual solutions
Stability analysis

ABSTRACT

The unsteady flow and heat transfer past a stretching/shrinking sheet in a hybrid nanofluid is studied. The governing equations of the problem are transformed to the similarity equations by using similarity transformation technique. The problem is solved numerically using the boundary value problem solver (bvp4c) in Matlab software. The plots of the skin friction coefficient and the local Nusselt number as well as the velocity and temperature profiles for selected parameters are presented. It is found that dual solutions exist for a certain range of the unsteadiness parameter. A temporal stability analysis is performed to determine the stability of the dual solutions in a long run, and it is reveals that only one of them is stable while the other is unstable.

1. Introduction

Nowadays, the problem of heat transfer enhancement is very important in engineering and industrial applications. Most of the applications using pure fluid as a cooling liquid such as water, ethylene glycol and oil which has low thermal conductivity, thus limits the heat transfer enhancement. However, new types of fluids such as nanofluids are introduced in order to get improvement in thermal efficiency. Nanofluids defined as a mixture containing dispersed nanometer sized particles and the base fluid which is first introduced by Choi [1] in order to develop advanced heat transfer fluids with substantially higher conductivities. He expected that the addition of metallic nanoparticles in the base fluids can essentially improve the thermal conductivities of the conventional base fluids and enhance the heat transfer execution of these fluids. Nanofluids are widely used as coolants, lubricants, and also in practical applications including refrigeration and air-conditioning, microelectronics, processors of mobile computers and etc. In recent years, the behaviour and characteristics of nanofluids in different problems have been studied experimentally and numerically by many researchers. For example, Hwang et al. [2] estimated thermal conductivities of different nanofluids and demonstrated that the thermal conductivity improvement of nanofluids relied upon the volume fraction of the suspended particles and the thermal conductivities of the particles and base fluids. An experimental investigation of nanofluid flow boiling heat transfer in a vertical tube under different pressure conditions has been studied by Wang and Su [3]. The flow boiling heat transfer of the AlN/H_2O nanofluid was studied experimentally by Wang et al. [4], where the nanofluid was prepared by modifying the nanoparticles into the deionized water and dissolving by an ultrasonic oscillation. Ahmadi and Willing [5] experimentally studied the heat transfer measurement in water based nanofluids and develop a CFD model using a Eulerian-Lagrange approach to study the nature of both the laminar and turbulent flow fields of the fluid and the dispersed nanoparticles.

In addition, the investigation on the mathematical models of nanofluid is reported by many researchers. There are two common types of nanofluid models that have been considered in fluid dynamics, namely the model proposed by Buongiorno [6] and Tiwari and Das [7]. The efficiency of the thermal conductivity of nanofluid among the models is examined in order to compare the theoretical data with the experimental data. Some researchers such as Nield and Kuznetsov [8], Kuznetsov and Nield [9], Khan and Pop [10], Khan and Aziz [11], Ahmad et al. [12], Rohni et al. [13], and Bachok et al. [14] used the mathematical nanofluid model proposed by Buongiorno [6], which takes into account the effects of Brownian motion and thermophoresis parameters. The nanofluid model proposed by Tiwari and Das [7] was also employed by

* Corresponding author.
E-mail address: popm.ioan@yahoo.co.uk (I. Pop).

https://doi.org/10.1016/j.ijheatmasstransfer.2019.02.101
0017-9310/

Nomenclature

a	constant
C_f	skin friction coefficient
C_p	specific heat at constant temperature
(ρC_p)	heat capacitance of the fluid
k	thermal conductivity
Nu_x	local Nusselt number
Re_x	local Reynolds number
p	fluid pressure
Pr	Prandtl number
q_w	surface heat flux
S	constant mass flux
T	fluid temperature
T_w	surface temperature
T_∞	ambient temperature
t	time
$u,\ v$	velocity component in the x and y directions
u_w	velocity of the stretching/shrinking sheet
u_∞	velocity of the mainstream
v_w	velocity of the wall mass transfer
$x,\ y$	Cartesian coordinates

Greek symbols

α	a parameter showing the unsteadiness of the problem
β	unsteadiness parameter
$\varphi_1,\ \varphi_2$	nanoparticle volume fractions for Al_2O_3 (alumina) and Cu (copper)
η	similarity variable
γ	eigenvalue
λ	stretching/shrinking parameter
θ	dimensionless temperature
μ	dynamic viscosity
ν	kinematic viscosity
ψ	stream function
ρ	fluid density
τ	dimensionless time variable
τ_w	wall shear stress

Subscripts

f	fluid
nf	nanofluid
hnf	hybrid nanofluid
$s1$	first solid component
$s2$	second solid component

Superscript

$'$	differentiation with respect to η

several authors such as Bachok et al. [15], Rohni et al. [16] and Das et al. [17]. It is worth mentioning that Wang and Wu [18] numerically studied the growth and departure of a single bubble behavior in Al_2O_3/H_2O nanofluid and pure water flow boiling process. The results indicate that the bubble in Al_2O_3/H_2O nanofluids grows faster and the bubble departure frequency of Al_2O_3/H_2O nanofluids is greater than that in pure water. The flow boiling heat flux is also improved by dispersing nanoparticles of Al_2O_3/H_2O in pure water. This work initially reveals that nanofluids can enhance flow boiling heat transfer from the point of view of bubble dynamics behavior.

However, researchers still eager to find a better type of fluid instead of nanofluid and it is in search until these recent years. To achieve the desire of getting better fluid which has the high thermal conductivity, some kind of nanofluids called 'hybrid nanofluids' are introduced. Hybrid nanofluid is an extension of nanofluid which composed of two different nanoparticles disperses in the base fluid. This kind of fluid is believed to offer good thermal characteristics as compared to the base fluid and nanofluid containing single nanoparticles. Hybrid nanofluids are widely applied in many fields of heat transfer such as electronic cooling, generator cooling, coolant in machining, nuclear system cooling, transformer cooling, biomedical, drug reduction, refrigeration and etc. with better efficiency compared to nanofluids applicability.

The capability of hybrid nanofluids in enhancing the thermal characteristics attracts the researchers to work towards hybrid nanofluid in real world heat transfer problems. For example, the synthesis of hybrid nano-composite particles, two different hybrid of polypyrrole-carbon nanotube (PPY-CNT) nano-composite and MWCNT on magnetic Fe_2O_3 nanoparticles were reported by Turcu et al. [19]. Moreover, Jana et al. [20] observed the enhancement of fluid thermal conductivity by the addition of single and hybrid nano-additives. The effect of Al_2O_3-Cu/water hybrid nanofluid in heat transfer was reported by Suresh et al. [21]. Synthesis of spherical silica/multiwall carbon nanotubes hybrid nanostructures and investigation of thermal conductivity of related nanofluids was analysed by Baghbanzadeha et al. [22]. Soltani and Akbari [23] studied the effects of temperature and particles concentration on the dynamic viscosity of MgO-MWCNT/EG hybrid nanofluid. Later, Vafaei et al. [24] predicted the thermal conductivity of MgO-MWCNTs/EG hybrid nanofluid at volume fractions of 0.05–0.6 percent and temperature 25–50 °C using several experimental methods.

Furthermore, numerical investigation on the effect of hybrid nanofluid in channel flows was studied by Yen et al. [25]. Labib et al. [26] was numerically investigated the problem on the effect of base fluids and hybrid nanofluid in forced convective heat transfer. The influence of nanofluid with double nanoparticles in a flat plate solar collector using finite element simulation was examined by Nasrin and Alim [27]. Takabi and Shokouhmand [28] conveyed the effects of Al_2O_3-Cu/water hybrid nanofluid on heat transfer and flow characteristics in turbulent regime. Devi and Devi [29] investigated the problem of three-dimensional hybrid Cu-Al_2O_3/water nanofluid flow over a stretching sheet with effecting Lorentz force subject to Newtonian heating. Later, Devi and Devi [30] studied the heat transfer enhancement of Cu-Al_2O_3/water hybrid nanofluid flow over a stretching sheet. Stagnation-point flow of an aqueous titania-copper hybrid nanofluid toward a wavy cylinder was investigated by Yousefi et al. [31]. Rotating flow of Ag-CuO/H_2O hybrid nanofluid with radiation and partial slip boundary effects was studied by Hayat et al. [32]. Recently, there are more numerical investigation involving hybrid nanofluids was studied by the researchers with different cases such as Ghadikolaei et al. [33], Tayebi and Chamkha [34], Ashorynejad and Shahriari [35], and Ghalambaz et al. [36].

There are many parameters that highly contribute to the heat transfer enhancement of hybrid nanofluid such as base fluid selection, nanoparticles size, viscosity, fluid temperature and stability, dispersibility of the nanoparticles, purity of nanoparticles, preparation method, size and shape of nanoparticles and compatibility of the nanoparticles that lead to harmonious mixture of the nanofluid (Li et al., [37]; Paul et al., [38]). For instance, the collection of papers on nanofluids or hybrid nanofluids can be found in the book by Das et al. [39] and in the review papers by Trisaksri and Wongwises [40], Wang and Mujumdar [41–43], Kakaç and

Pramuanjaroenkij [44], Kamyar et al. [45], Sarkar et al. [46], Akilu et al. [47], Babu et al. [48], Leong et al. [49], Ahmadi et al. [50], Ali et al. [51], Huminic and Huminic [52], Sidik et al. [53], and Sundar et al. [54].

The fluid dynamics due to a stretching sheet has important applications in industries such as the hot rolling, wire drawing, and glass-fibre production. In view of these applications, Sakiadis [55] first investigated the boundary layer flow on a continuous solid surface moving at constant speed. Since the pioneering study by Crane [56], who presented an exact analytical solution for the steady two-dimensional flow due to a stretching surface in a quiescent fluid, many authors have considered various aspects of this problem and obtained similarity solutions such as Chen and Char [57], Wang [58], Andersson and Dandapat [59], Gorla and Sidawi [60], Chen [61], Magyari and Keller [62], Andersson [63], and Ishak et al. [64,65]. However, instead of considering the case of stretching sheet, researchers also investigated the case of shrinking sheet. This new type of shrinking sheet flow is essentially a backward flow as discussed by Goldstein [66]. The development of the unusual type of flow due to shrinking was first observed by Wang [67] when he investigated the behaviour of a liquid film on an unsteady stretching sheet. Miklavčič and Wang [68] investigated the steady flow over a shrinking sheet, which is an exact solution of the Navier-Stokes equations and found that mass suction is required to maintain the flow over a shrinking sheet. The flow induced by a shrinking sheet with constant velocity or power-law velocity distribution was investigated by Fang et al. [69,70], Fang [71] and Fang and Zhang [72]. According to Fang et al. [70], the flow induced by a shrinking sheet shows physical phenomena quite distinct from the forward stretching flow. The shrinking sheet problem was also extended to other fluids and various geometry with different conditions by many researchers such as Hayat et al. [73], Sajit et al. [74], Wang [75], Merkin and Kumaran [76], Bhattacharyya [77,78], Yacob and Ishak [79], Awaludin et al. [80], Soid et al. [81] and Pop et al. [82]. The problem of shrinking sheet immersed in nanofluids for three types of nanoparticles which are copper, alumina and Titania by considering water as the based fluid was solved numerically by Rohni et al. [16].

Motivated by the above studies, the present paper aims to investigate the problem of the unsteady flow and heat transfer of a hybrid nanofluid past a stretching/shrinking sheet with wall mass suction by employing nanofluid equations model proposed by Tiwari and Das [7]. Hybrid nanofluid is considered by suspending two different nanoparticles which are Al_2O_3 and Cu in pure water. The governing equations with boundary conditions are transformed into a system of ordinary differential equations by using a similarity transformation. The system of equations is then solved numerically using the boundary value problem solver (bvp4c) in Matlab software. The effects of several parameters on the flow and heat transfer characteristics are presented in graphical form. To validate the numerical results obtained, the comparison has been made with the existing results in the literature. To the present knowledge of the authors, no studies have been reported in the literature, which investigated the flow over a shrinking sheet in hybrid nanofluids.

2. Mathematical formulation

Let us consider the two-dimensional, laminar boundary layer flow of an incompressible, and unsteady flow of a hybrid nanofluid past a stretching/shrinking sheet as shown in Fig. 1, where the x and y are dimensional Cartesian coordinates with the x-axis measured along the surface and y-axis normal to it, respectively, the surface being located in the plane $y = 0$. It is assumed that the velocity of the stretching/shrinking sheet is $u_w(x,t) = U_w(x)/(1-\alpha t)$, where t is time, α is a parameter showing the unsteadiness of the problem, the wall mass suction velocity is $v_w(x,t)$, which will be determined later and $U_w(x) = ax$, a being a positive constant. Physically, value of $\alpha > 0$ accelerates the outer potential flow and $\alpha < 0$ does the reverse flow, while $\alpha = 0$ corresponds to the steady inviscid flow.

It is also assumed that the base fluid (i.e. water) and the nanoparticles are in thermal equilibrium and no slip occurs between them. Therefore, by using the nanofluid model as proposed by Tiwari and Das [7], the governing equations of this problem in Cartesian coordinates x and y are (see Rohni et al. [16]; Devi and Devi [30]; Fang et al. [70]),

$$\frac{\partial u}{\partial x} + \frac{\partial v}{\partial y} = 0 \tag{1}$$

$$\frac{\partial u}{\partial t} + u\frac{\partial u}{\partial x} + v\frac{\partial u}{\partial y} = -\frac{1}{\rho_{hnf}}\frac{\partial p}{\partial x} + \frac{\mu_{hnf}}{\rho_{hnf}}\nabla^2 u \tag{2}$$

$$\frac{\partial v}{\partial t} + u\frac{\partial v}{\partial x} + v\frac{\partial v}{\partial y} = -\frac{1}{\rho_{hnf}}\frac{\partial p}{\partial y} + \frac{\mu_{hnf}}{\rho_{hnf}}\nabla^2 v \tag{3}$$

$$\frac{\partial T}{\partial t} + u\frac{\partial T}{\partial x} + v\frac{\partial T}{\partial y} = \frac{k_{hnf}}{(\rho C_p)_{hnf}}\nabla^2 T \tag{4}$$

subject to the initial and boundary conditions,

$$\begin{aligned} &t < 0: \quad v = 0, \quad u = 0, \quad T = T_\infty \text{ for any } x, y \\ &t \geqslant 0: \quad v = v_w(x,t), \quad u = \lambda u_w(x,t), \quad T = T_w \quad \text{at} \quad y = 0 \\ &u \to 0, \quad T \to T_\infty \quad \text{as} \quad y \to \infty \end{aligned} \tag{5}$$

where u and v are velocity components along the axes x and y, T is the temperature of the hybrid nanofluid, p is the pressure, $\nabla^2 = \partial^2/\partial x^2 + \partial^2/\partial y^2$ is the Laplacian, λ is the constant stretching/shrinking parameter with $\lambda > 0$ for a stretching sheet, $\lambda < 0$ for a shrinking sheet and $\lambda = 0$ for a static surface, μ_{hnf} is the dynamic viscosity, k_{hnf} is the thermal conductivity, ρ_{hnf} is the density and $(\rho C_p)_{hnf}$ is the heat capacity of the hybrid nanofluid.

Following Devi and Devi [30], a special form of thermophysical properties are introduced in the present study to analyze the unsteady boundary layer equations for hybrid nanofluid, which is considered by taking the mixture of Cu nanoparticles into 0.1 volume of Al_2O_3/water to form the required hybrid nanofluid. In this model, initially the nanoparticle of Al_2O_3 (φ_1) is added to the base fluid with 0.1 volume solid volume fraction (i.e. $\varphi_1 = 0.1$), which is fixed throughout the problem hereafter and consequently Cu (φ_2) is added with various solid volume fractions to form the hybrid nanofluid namely Cu-Al_2O_3/water. To make it clear, the final form of the effective thermophysical properties of nanofluid and hybrid nanofluid are given in Table 1. The thermophysical properties of fluid and nanoparticles are provided in Table 2.

3. Solution for the steady-state flow ($\partial/\partial t = 0$)

To obtain the similarity solutions for the system of Eqs. (1)–(4) subject to the boundary conditions (5), we use the following similarity transformation (see Fang et al. [70]),

$$\psi = x\sqrt{\frac{a\nu_f}{1-\alpha t}}f(\eta), \quad \theta(\eta) = \frac{T - T_\infty}{T_w - T_\infty}, \quad \eta = y\sqrt{\frac{a}{\nu_f(1-\alpha t)}} \tag{6}$$

where ψ is the stream function that satisfies Eq. (1), and the velocity components are defined as $u = \partial\psi/\partial y$ and $v = -\partial\psi/\partial x$. With these definitions, the velocities are expressed as

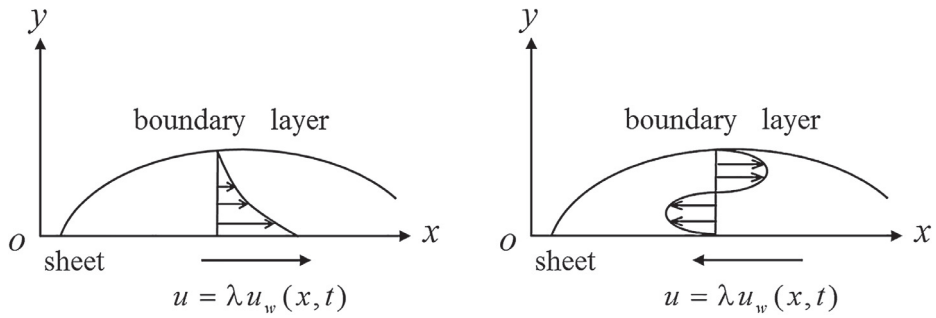

Fig. 1. Physical models and coordinate systems.

Table 1
Thermophysical properties of nanofluid and hybrid nanofluid (see Devi and Devi [29]; Yousefi et al. [30]; Khanafer et al. [82]; Oztop and Abu-Nada [83]).

Properties	Nanofluid	Hybrid Nanofluid
Density	$\rho_{nf} = (1-\varphi_1)\rho_f + \varphi_1\rho_{s1}$	$\rho_{hnf} = (1-\varphi_2)[(1-\varphi_1)\rho_f + \varphi_1\rho_{s1}] + \varphi_2\rho_{s2}$
Heat capacity	$(\rho C_p)_{nf} = (1-\varphi_1)(\rho C_p)_f + \varphi_1(\rho C_p)_{s1}$	$(\rho C_p)_{hnf} = (1-\varphi_2)[(1-\varphi_1)(\rho C_p)_f + \varphi_1(\rho C_p)_{s1}] + \varphi_2(\rho C_p)_{s2}$
Dynamic viscosity	$\mu_{nf} = \frac{\mu_f}{(1-\varphi_1)^{2.5}}$	$\mu_{hnf} = \frac{\mu_f}{(1-\varphi_1)^{2.5}(1-\varphi_2)^{2.5}}$
Thermal conductivity	$k_{nf} = \frac{k_{s1}+2k_f-2\varphi_1(k_f-k_{s1})}{k_{s1}+2k_f+\varphi_1(k_f-k_{s1})} \times (k_f)$	$k_{hnf} = \frac{k_{s2}+2k_{nf}-2\varphi_2(k_{nf}-k_{s2})}{k_{s2}+2k_{nf}+\varphi_2(k_{nf}-k_{s2})} \times (k_{nf})$ where $k_{nf} = \frac{k_{s1}+2k_f-2\varphi_1(k_f-k_{s1})}{k_{s1}+2k_f+\varphi_1(k_f-k_{s1})} \times (k_f)$

Table 2
Thermophysical properties of fluid and nanoparticles (see Rohni et al. [16]; Oztop and Abu-Nada [84]).

Physical properties	Fluid phase (water)	Al_2O_3	Cu
ρ (kg/m^3)	997.1	3970	8933
C_p (J/kgK)	4179	765	385
k (W/mK)	0.613	40	400

$$u = \frac{ax}{1-\alpha t} f'(\eta), \qquad v = -\sqrt{\frac{av_f}{1-\alpha t}} f(\eta) \tag{7}$$

The pressure term can be integrated from Eq. (3). Then the wall mass transfer velocity becomes

$$v_w(x,t) = -\sqrt{\frac{av_f}{1-\alpha t}} S \tag{8}$$

where S is the constant mass flux velocity with $S > 0$ for suction and $S < 0$ for injection.

Substituting (6) into Eqs. (2) and (4), one obtains the following nonlinear ordinary differential equations:

$$f''' + (1-\varphi_1)^{2.5}(1-\varphi_2)^{2.5} \times \left\{(1-\varphi_2)\left[(1-\varphi_1) + \varphi_1\left(\frac{\rho_{s1}}{\rho_f}\right)\right] + \varphi_2\left(\frac{\rho_{s2}}{\rho_f}\right)\right\} \times \left[ff'' - f'^2 - \beta\left(f' + \frac{\eta}{2}f''\right)\right] = 0 \tag{9}$$

$$\theta'' + \Pr\left(\frac{k_f}{k_{hnf}}\right)\left\{(1-\varphi_2)\left[(1-\varphi_1) + \varphi_1\frac{(\rho C_p)_{s1}}{(\rho C_p)_f}\right] + \varphi_2\frac{(\rho C_p)_{s2}}{(\rho C_p)_f}\right\} \times \left[f\theta' - \frac{\beta}{2}\eta\theta'\right] = 0 \tag{10}$$

subject to the boundary conditions

$$f(0) = S, \quad f'(0) = \lambda, \quad \theta(0) = 1$$
$$f'(\eta) \to 0, \quad \theta(\eta) \to 0 \ \text{ as } \ \eta \to \infty \tag{11}$$

where prime denotes differentiation with respect to η and $\beta = \alpha/a$ is the unsteadiness parameter, with $\beta > 0$ for accelerating flow and $\beta < 0$ for decelerating flow. For the present study, we assume a decelerating stretching/shrinking sheet with $\beta \leqslant 0$. We notice that when $\varphi_1 = \varphi_2 = 0$, Eq. (9) reduces to Eq. (6) of Fang et al. [70] as rewrite in the following Eq. (12):

$$f''' + ff'' - f'^2 - \beta\left(f' + \frac{\eta}{2}f''\right) = 0 \tag{12}$$

The physical quantities of interest are the skin friction coefficient C_f and the local Nusselt number Nu_x, which are defined as

$$C_f = \frac{\tau_w}{\rho_f U_w^2}, \qquad Nu_x = \frac{xq_w}{k_f(T_w - T_\infty)} \tag{13}$$

where τ_w is the skin friction or shear stress along the sheet and q_w is the heat flux from the sheet, that are given by

$$\tau_w = \mu_{hnf}\left(\frac{\partial u}{\partial y}\right)_{y=0}, \qquad q_w = -k_{hnf}\left(\frac{\partial T}{\partial y}\right)_{y=0} \tag{14}$$

Substituting (6) into (14) and using (13), one gets

$$C_f Re_x^{1/2} = \frac{1}{(1-\varphi_1)^{2.5}(1-\varphi_2)^{2.5}} f''(0),$$
$$Nu_x Re_x^{-1/2} = -\frac{k_{hnf}}{k_f}\theta'(0) \tag{15}$$

where $Re_x = u_w x/\nu_f$ is the local Reynolds number.

4. Stability analysis

It has been established by Merkin [85], Weidman et al. [86], Roşca and Pop [87,88] and Harris et al. [89] for different problems, that the basic ordinary (similarity) equations admit multiple (dual)

solutions, where the upper branch solutions are stable, while the lower branch solutions are unstable. We test these features by considering the boundary value problem of Eqs. (9)–(11). Thus, we introduce the new dimensionless time variable $\tau = at/(1-\alpha t)$. Using variables in (6) and (7), we have

$$u(x,\tau) = \frac{ax}{1-\alpha t}\frac{\partial f}{\partial \eta}(\eta,\tau), \quad v = -\sqrt{\frac{av_f}{1-\alpha t}}f(\eta,\tau),$$
$$\theta(\eta,\tau) = \frac{T-T_\infty}{T_w-T_\infty}, \quad \eta = y\sqrt{\frac{a}{\nu_f(1-\alpha t)}}, \quad \tau = \frac{at}{1-\alpha t} \tag{16}$$

Using (16), Eqs. (9) and (10) can be written as

$$\frac{\partial^3 f}{\partial \eta^3} + (1-\varphi_1)^{2.5}(1-\varphi_2)^{2.5}\left\{(1-\varphi_2)\left[(1-\varphi_1)+\varphi_1\left(\frac{\rho_{s1}}{\rho_f}\right)\right]+\varphi_2\left(\frac{\rho_{s2}}{\rho_f}\right)\right\} \times\left[f\frac{\partial^2 f}{\partial \eta^2}-\left(\frac{\partial f}{\partial \eta}\right)^2-\beta\left(\frac{\partial f}{\partial \eta}+\frac{\eta}{2}\frac{\partial^2 f}{\partial \eta^2}\right)-\frac{\partial^2 f}{\partial \eta \partial \tau}\right]=0 \tag{17}$$

$$\frac{\partial^2 \theta}{\partial \eta^2}+\Pr\left(\frac{k_f}{k_{hnf}}\right)\left\{(1-\varphi_2)\left[(1-\varphi_1)+\varphi_1\frac{(\rho C_p)_{s1}}{(\rho C_p)_f}\right]+\varphi_2\frac{(\rho C_p)_{s2}}{(\rho C_p)_f}\right\} \times\left[f\frac{\partial \theta}{\partial \eta}-\frac{\beta}{2}\eta\frac{\partial \theta}{\partial \eta}-\frac{\partial \theta}{\partial \tau}\right]=0 \tag{18}$$

and the boundary conditions (11) become

$$f(0,\tau)=S, \quad \frac{\partial f}{\partial \eta}(0,\tau)=\lambda, \quad \theta(0,\tau)=1$$
$$\frac{\partial f}{\partial \eta}(\eta,\tau)\to 0, \quad \theta(\eta,\tau)\to 0 \ \text{ as } \ \eta\to\infty \tag{19}$$

To determine the stability of the steady flow solution $f=f_0(\eta)$ and $\theta=\theta_0(\eta)$ satisfying the boundary value problem (9)–(11), we write (see Merkin [85], Weidman et al. [86] and Roşca and Pop [87,88])

$$f(\eta,\tau)=f_0(\eta)+e^{-\gamma\tau}F(\eta), \qquad \theta(\eta,\tau)=\theta_0(\eta)+e^{-\gamma\tau}G(\eta) \tag{20}$$

where γ is an unknown eigenvalue parameter, and functions $F(\eta)$ and $G(\eta)$ are small relative to $f_0(\eta)$ and $\theta_0(\eta)$. Substituting Eq. (20) into Eqs. (17) and (18) along with the boundary conditions (19), the following linear eigenvalue problem are obtained:

$$F'''+(1-\varphi_1)^{2.5}(1-\varphi_2)^{2.5}\left\{(1-\varphi_2)\left[(1-\varphi_1)+\varphi_1\left(\frac{\rho_{s1}}{\rho_f}\right)\right]+\varphi_2\left(\frac{\rho_{s2}}{\rho_f}\right)\right\} \times\left[f_0F''+Ff_0''-2f_0'F'-\beta\left(F'+\frac{\eta}{2}F''\right)+\gamma F'\right]=0 \tag{21}$$

$$G''+\Pr\left(\frac{k_f}{k_{hnf}}\right)\left\{(1-\varphi_2)\left[(1-\varphi_1)+\varphi_1\frac{(\rho C_p)_{s1}}{(\rho C_p)_f}\right]+\varphi_2\frac{(\rho C_p)_{s2}}{(\rho C_p)_f}\right\} \times\left[f_0G'+F\theta_0'-\frac{\beta}{2}\eta G'+\gamma G\right]=0 \tag{22}$$

and the boundary conditions (19) become

$$F(0)=0, \quad F'(0)=0, \quad G(0)=0$$
$$F'(\eta)\to 0, \quad G(\eta)\to 0 \ \text{ as } \ \eta\to\infty \tag{23}$$

Solving the eigenvalue problems (21)–(23) one obtains an infinite number of eigenvalues $\gamma_1<\gamma_2<\gamma_3<\ldots$ If the smallest eigenvalue γ is positive the flow is stable and if the smallest eigenvalue γ is negative the flow is unstable.

5. Results and discussion

Numerical solutions of the nonlinear ordinary differential equations (9) and (10) along with the boundary conditions (11) were obtained using the boundary value problem solver (bvp4c) in Matlab software. The solutions are obtained using an initial guess supplied at an initial mesh point and changes step size to get the specified accuracy. The details of this method can be found in Shampine et al. [90]. The suitable initial guess and the boundary layer thickness, η_∞ must be chosen depending on the values of the parameters used. To solve this boundary value problem, it is necessary to first reduce the equations to a system of first order ordinary differential equations.

Validation of the numerical procedure is obtained by comparing the numerical results of the present study with the numerical results from the previous study for different cases as shown in Tables 3–5. Table 3 displays the values of $-\theta'(0)$ for regular fluid ($\varphi_1=0$, $\varphi_2=0$) with various values of Pr when $S=0$, $\beta=0$, and $\lambda=1$ (stretching sheet). It is observed that the present results are in a good agreement with the solutions obtained by Khan and Pop [10], Devi and Devi [30], Wang [58] and Gorla and Sidawi [60] for regular fluid case.

Meanwhile, Table 4 shows the values of $f''(0)$ and $-\theta'(0)$ for Cu–water nanofluid ($\varphi_1=0$, $\varphi_2=0.2$) with various values of β when $S=2.1$, $\Pr=6.2$ and $\lambda=-1$ (shrinking sheet). We notice that by setting $\varphi_1=0$ in Eq. (9), the equation reduces to Eq. (9) of Rohni et al. [16]. The present numerical values of $f''(0)$ are compared to the solutions obtained by Rohni et al. [16], which shows a good agreement.

The values of $C_fRe_x^{1/2}$ and $Nu_xRe_x^{-1/2}$ for Cu-Al_2O_3/water hybrid nanofluid with various values of φ_2 when $\phi_1=0.1$, $S=0$, $\beta=0$, $\Pr=6.135$ and $\lambda=1$ (stretching sheet) are given in Table 5. Following Devi and Devi [30], the thermophysical properties of fluid (water) at 25 °C are used for this particular results where $\rho_f=997$, $(C_p)_f=4180$ and $k_f=0.6071$. The comparison shows a favorable agreement with the results obtained by Devi and Devi [30].

The variations of $f''(0)$ and $-\theta'(0)$ for different values of parameters are presented in Figs. 2–7. We notice from these figures that dual solutions exist with upper and lower branch solutions for a certain range of the unsteadiness parameter β. As mentioned previously, we assume a decelerating stretching/shrinking sheet with $\beta\leqslant 0$. The dual solutions only exist when the value of β is equal to a certain critical value β_c. The critical value β_c is the value where the upper branch solution meets the lower branch solution. There is no similarity solutions exist beyond this critical values due to the boundary layer separates from the surface and the solution based upon the boundary layer approximations are not possible.

In detail, Figs. 2 and 3 displays the variation of $f''(0)$ and $-\theta'(0)$ with β for various values of S when $\Pr=6.2$ and $\lambda=-1$ in regular fluid ($\varphi_1=0$, $\varphi_2=0$). We observed that with the increase of S, the solution domain expands with the critical values β_c moving to the left. Based on our computations, the critical value of β for the suction parameter $S=2.1$, 2.15, and 2.2 are $\beta_c=-1.6556$, -8.8840 and -8.3490, respectively. Meanwhile, for $S=2.5$ we aspect that the critical value is smaller than those of $S=2.1$, 2.15, and 2.2. This implies that the increment of S delays the boundary layer separation. In addition, the values of $f''(0)$ is increases with the increasing of S for the upper branch solution while it is decreases for the lower branch solution. The increasing of S leads to enhance the values of $-\theta'(0)$ for both branches.

Figs. 4 and 5 illustrate the variation of $f''(0)$ and $-\theta'(0)$ with β for various values of φ_1 and φ_2 when $\Pr=6.2$, $\lambda=-1$ and $S=2.2$. It can be seen that the critical values β_c for the regular fluid ($\varphi_1=\varphi_2=0$) is a bit smaller than the critical values β_c for the nanofluid ($\varphi_1=0.1$, $\varphi_2=0$) which are $\beta_c=-8.3490$ and $\beta_c=-8.0118$, respectively. However, for the case of hybrid nanofluid ($\varphi_1=0.1$, $\varphi_2=0.1$) the critical values β_c is moving more to the negative value of β.

Variations of $f''(0)$ and $-\theta'(0)$ with β for various values of φ_2 when $\Pr=6.2$, $\lambda=-1$, $S=2.2$ and $\varphi_1=0.1$ are plotted in Figs. 6

Table 3
Values of $-\theta'(0)$ for regular fluid ($\varphi_1 = 0$, $\varphi_2 = 0$) with various values of Pr when $S = 0$, $\beta = 0$, and $\lambda = 1$.

Pr	Khan and Pop [10]	Devi and Devi [30]	Wang [58]	Gorla and Sidawi [60]	Present results
2	0.9113	0.91135	0.9114	0.9114	0.911353
6.13	–	1.75968	–	–	1.759682
7	1.8954	1.89540	1.8954	1.8954	1.895400
20	3.3539	3.35390	3.3539	3.3539	3.353902

Table 4
Values of $f''(0)$ and $-\theta'(0)$ for Cu–water nanofluid ($\varphi_1 = 0$, $\varphi_2 = 0.2$) with various values of β when $S = 2.1$, $\lambda = -1$ and Pr = 6.2 (water).

β	$f''(0)$				$-\theta'(0)$	
	Rohni et al. [16]		Present results		Present results	
	First solution	Second solution	First solution	Second solution	First solution	Second solution
0	2.5290	0.5847	2.528984	0.584729	6.822454	6.693105
−0.2	2.4621	−0.0481	2.462145	−0.048071	6.875796	6.716536
−0.4	2.3953	−0.4735	2.395252	−0.473472	6.927417	6.755470
−0.6	2.3283	−0.8408	2.328304	−0.840776	6.977507	6.797695
−1	2.1942	−1.4913	2.194247	−1.491281	7.073680	6.884548
−3	1.5212	−4.1448	1.521197	−4.144746	7.497151	7.296176
−5	0.8444	−6.4315	0.844435	−6.431507	7.858446	7.657801
−9	−0.5173	−10.5898	−0.517287	−10.589830	8.473316	8.277676

Table 5
Values of $C_{fx}Re_x^{1/2}$ and $Nu_xRe_x^{-1/2}$ for Cu–Al_2O_3/water hybrid nanofluid with various values of φ_2 when $\varphi_1 = 0.1$, $S = 0$, $\beta = 0$, $\lambda = 1$ and Pr = 6.135.

φ_2	$C_{fx}Re_x^{1/2}$		$Nu_xRe_x^{-1/2}$	
	Devi and Devi [30]	Present results	Devi and Devi [30]	Present results
0.005	−1.327310	−1.327098	1.961686	1.961773
0.02	−1.409683	−1.409490	1.989226	1.989308
0.04	−1.520894	−1.520721	2.026368	2.026446
0.06	−1.634279	−1.634119	2.064075	2.064150

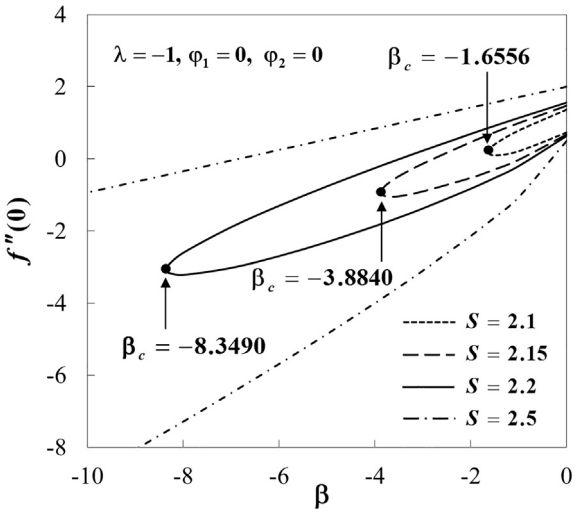

Fig. 2. Variation of $f''(0)$ with β for various values of S. when $\lambda = -1$, $\varphi_1 = 0$ and $\varphi_2 = 0$.

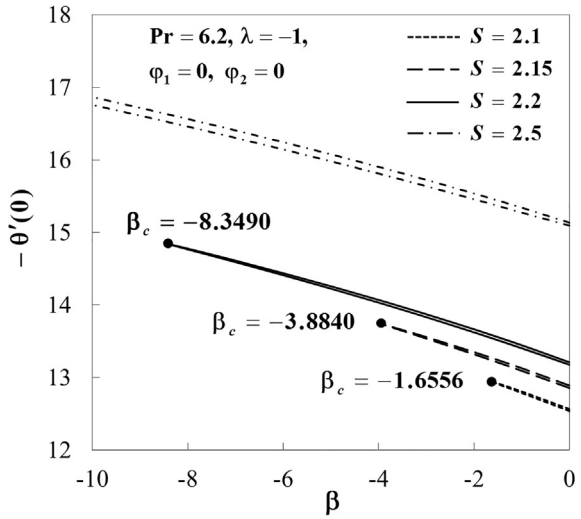

Fig. 3. Variation of $-\theta'(0)$ with β for various values of S. when Pr = 6.2, $\lambda = -1$, $\varphi_1 = 0$ and $\varphi_2 = 0$.

and 7. From these figures, it is shows that the critical value of β is getting smaller with the increasing of solid volume fraction φ_2. We can see that the critical value $\beta_c = -8.4795$ and $\beta_c = -13.8770$ for solid volume fraction $\varphi_2 = 0.001$ and $\varphi_2 = 0.01$, respectively. When the values of the solid volume fraction φ_2 get larger, the critical value of β become smaller that causes the extension of the boundary layer separation. Besides, the effects of φ_2 on the values of $f''(0)$ and $-\theta'(0)$ also can be observed in Figs. 6 and 7. We can see that the increasing of φ_2 enhances the values of $f''(0)$ for the upper branch solution while it is declines for the lower branch solution. Meanwhile, the values of $-\theta'(0)$ reduces with the increasing of φ_2 for both branches.

The velocity profiles $f'(\eta)$ and the temperature profiles $\theta(\eta)$ for various values of φ_2 when Pr = 6.2, $\lambda = -1$, $\beta = -2$, $S = 2.2$ and $\varphi_1 = 0.1$ are shown in Figs. 8 and 9. These figures show that there exist two different profiles for a particular values of solid volume fraction φ_2. It is found that the increasing of φ_2 leads to the increment of the fluid velocity and fluid temperature for the upper

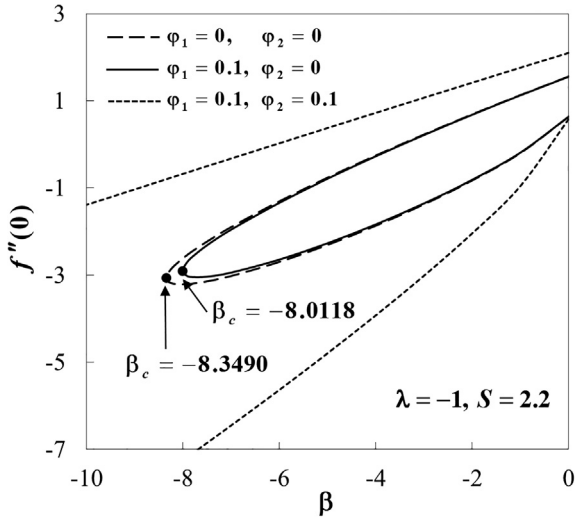

Fig. 4. Variation of $f''(0)$ with β for various values of φ_1 and φ_2. when $\lambda = -1$ and $S = 2.2$.

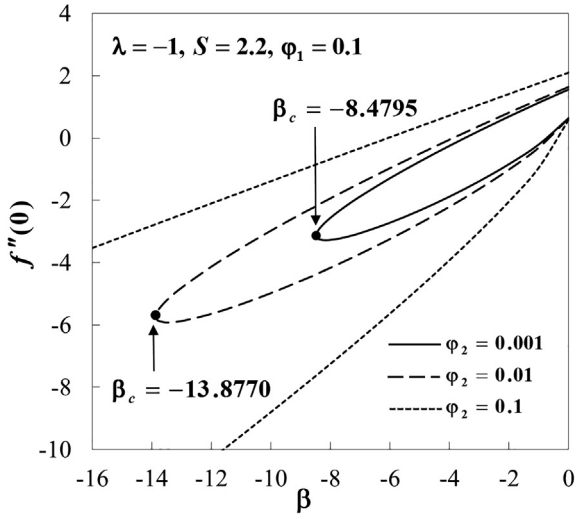

Fig. 6. Variation of $f''(0)$ with β for various values of φ_2 when. $\lambda = -1$, $S = 2.2$ and $\varphi_1 = 0.1$.

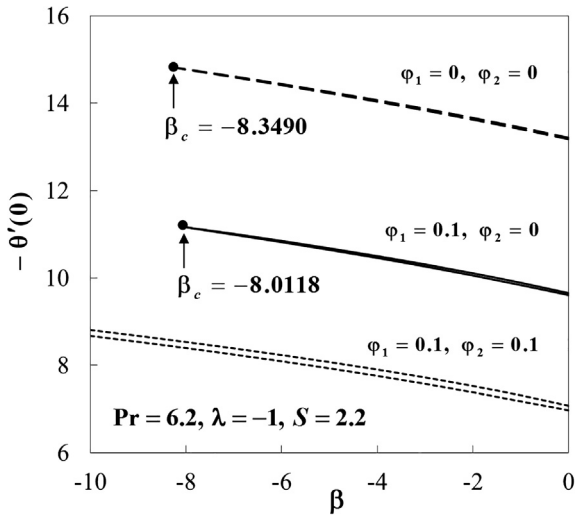

Fig. 5. Variation of $-\theta'(0)$ with β for various values of φ_1 and φ_2. when Pr = 6.2, $\lambda = -1$ and $S = 2.2$.

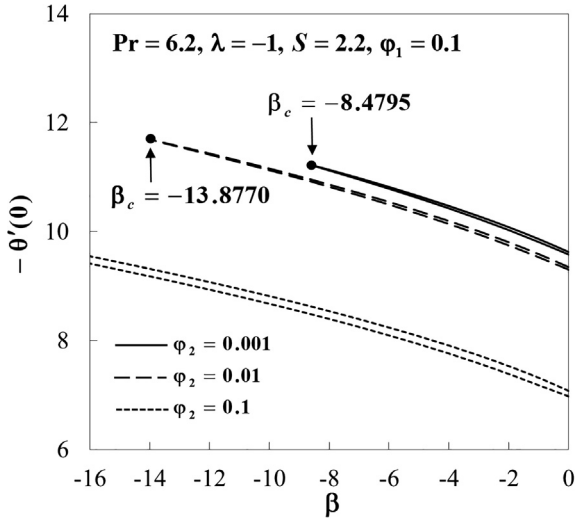

Fig. 7. Variation of $-\theta'(0)$ with β for various values of φ_2. when Pr = 6.2, $\lambda = -1$, $S = 2.2$ and $\varphi_1 = 0.1$.

branch. Meanwhile, fluid velocity decreases but fluid temperature increases for the lower branch with the increasing of φ_2.

Figs. 10 and 11 demonstrate the velocity profiles $f'(\eta)$ and the temperature profiles $\theta(\eta)$ for various values of S when Pr = 6.2, $\lambda = -1$, $\beta = -2$, $\varphi_1 = 0.1$ and $\varphi_2 = 0.1$. Note that the rise in the suction parameter S increases the fluid velocity but decreases the fluid temperature for the upper branch. For the lower branch, it is noticed that the fluid velocity and the fluid temperature decrease with increasing of the suction parameter S.

The smallest eigenvalues γ for various values of β when Pr = 6.2, $\lambda = -1$, $S = 2.2$, $\varphi_1 = 0.1$ and $\varphi_2 = 0.01$ are depicted in Fig. 12. This figure indicates that the negative value of γ refers to an initial growth of disturbance, and the flow is in unstable mode. Meanwhile, the positive value of γ denotes an initial decay of disturbance, and the flow is said to be in a stable mode. We can observe that the smallest eigenvalue γ tends to zero either from the upper branch or the lower branch as the values of β are approaching β_c. This shows that the transitions from positive (stable) to negative (unstable) of γ occur at the turning points.

6. Conclusions

The problem of the unsteady flow and heat transfer past a stretching/shrinking sheet in a hybrid nanofluid is investigated. The effects of the solid volume fraction φ_2, suction parameter S and unsteadiness parameter β on the velocity and temperature profiles, skin friction coefficient and local Nusselt number were presented graphically and discussed. Results demonstrated that the enhancement of the skin friction coefficient and reduction of the local Nusselt number on the shrinking sheet is observed with the increasing of φ_2 for the upper branch solution. Meanwhile, the values of the skin friction coefficient and the local Nusselt number declines with the increasing of φ_2 for the lower branch solution. The fluid velocity and fluid temperature for the upper branch increase, while fluid velocity decreases but fluid temperature increases for the lower branch with the increasing of φ_2. The suction parameter S increases the fluid velocity for the upper branch while it decreases for the lower branch. It is noticed that the fluid temperature decreases with the increasing of suction parameter S for both branches. We also observed that dual

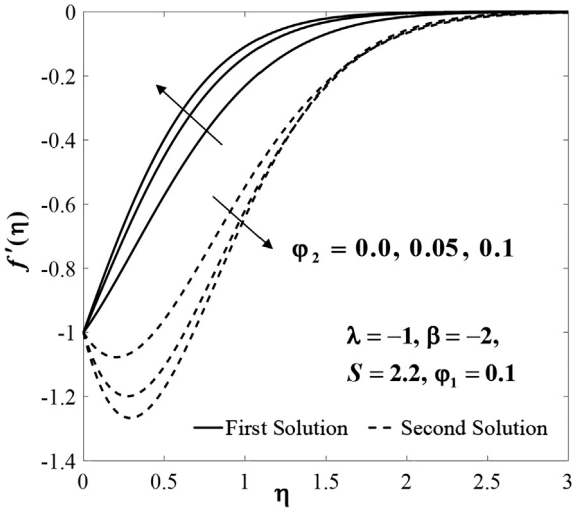

Fig. 8. The velocity profiles $f'(\eta)$ for various values of φ_2 when. $\lambda = -1$, $\beta = -2$, $S = 2.2$ and $\varphi_1 = 0.1$.

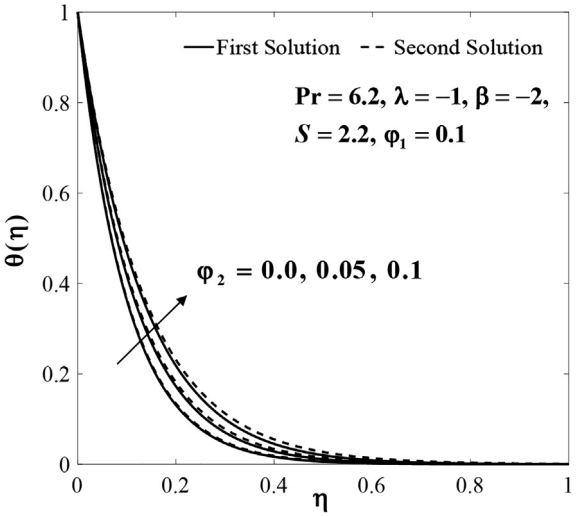

Fig. 9. The temperature profiles $\theta(\eta)$ for various values of φ_2 when Pr = 6.2, $\lambda = -1$, $\beta = -2$, $S = 2.2$ and $\varphi_1 = 0.1$.

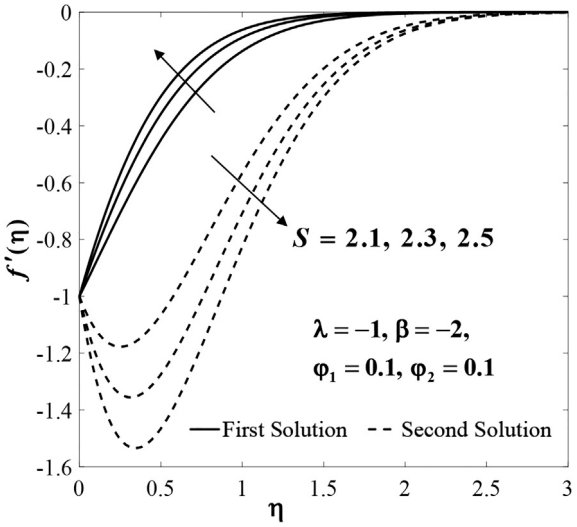

Fig. 10. The velocity profiles $f'(\eta)$ for various values of S when $\lambda = -1$, $\beta = -2$, $\varphi_1 = 0.1$ and $\varphi_2 = 0.1$.

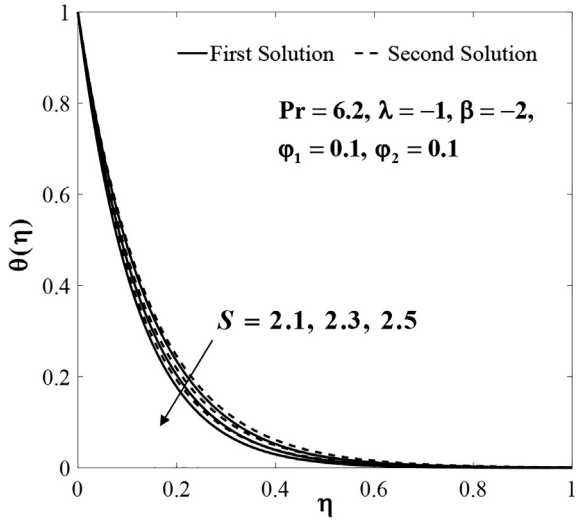

Fig. 11. The temperature profiles $\theta(\eta)$ for various values of S when Pr = 6.2, $\lambda = -1$, $\beta = -2$, $\varphi_1 = 0.1$ and $\varphi_2 = 0.1$.

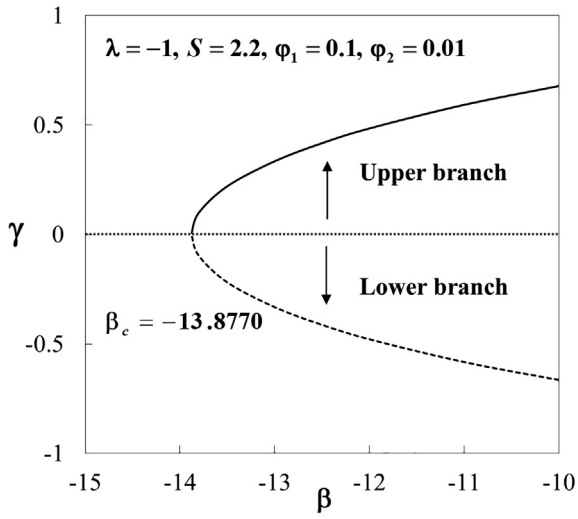

Fig. 12. Smallest eigenvalues γ for various values of β when $\lambda = -1$, $S = 2.2$, $\varphi_1 = 0.1$ and $\varphi_2 = 0.01$.

solutions exist for a certain range of the unsteadiness parameter β. Since the dual solutions exist, a stability analysis was conducted to determine the stability of the solutions. The stability analysis has confirmed that the upper branch solution is stable, while the lower branch solution is unstable.

Acknowledgements

The financial supports received from the Universiti Kebangsaan Malaysia (Project Code: GUP-2018-153), Universiti Teknikal Malaysia Melaka and the Ministry of Education, Malaysia are gratefully acknowledged. The work of Ioan Pop was supported by the grant PN-III-P4-ID-PCE-2016-0036, UEFISCDI of Romanian Ministry of Sciences. The authors also wish to express their thanks to the very competent Reviewers for their very good comments and suggestions.

Conflict of interest

There is no any conflict of interest between the authors of this paper.

Appendix A. Supplementary material

Supplementary data to this article can be found online at https://doi.org/10.1016/j.ijheatmasstransfer.2019.02.101.

References

[1] S.U.S. Choi, Enhancing thermal conductivity of fluids with nanoparticles, ASME Fluids Eng. Div. 231 (1995) 99–105.
[2] K.S. Hwang, J.H. Lee, S.P. Jang, Buoyancy-driven heat transfer of water-based Al_2O_3 nanofluids in a rectangular cavity, Int. J. Heat Mass Transfer 50 (2007) 4003–4010.
[3] Y. Wang, G.H. Su, Experimental investigation on nanofluid flow boiling heat transfer in a vertical tube under different pressure conditions, Exp. Therm. Fluid Sci. 77 (2016) 116–123.
[4] Y. Wang, K.H. Deng, B. Liu, J.M. Wu, G.H. Su, A correlation of nanofluid flow boiling heat transfer based on the experimental results of AlN/H_2O and Al_2O_3/H_2O nanofluid, Exp. Therm. Fluid Sci. 80 (2017) 376–383.
[5] M. Ahmadi, G. Willing, Heat transfer measurement in water based nanofluids, Int. J. Heat Mass Transfer 118 (2018) 40–47.
[6] J. Buongiorno, Convective transport in nanofluids, ASME J. Heat Trans. 128 (2006) 240–250.
[7] R.K. Tiwari, M.K. Das, Heat transfer augmentation in a two-sided lid-driven differentially heated square cavity utilizing nanofluids, Int. J. Heat Mass Transfer 50 (2007) 2002–2018.
[8] D.A. Nield, A.V. Kuznetsov, The Cheng-Minkowycz problem for natural convective boundary-layer flow in a porous medium saturated by a nanofluid, Int. J. Heat Mass Transfer 52 (2009) 5792–5795.
[9] A.V. Kuznetsov, D.A. Nield, Natural convective boundary-layer flow of a nanofluid past a vertical plate, Int. J. Therm. Sci. 49 (2010) 243–247.
[10] W. Khan, I. Pop, Boundary-layer flow of a nanofluid past a stretching sheet, Int. J. Heat Mass Transfer 53 (2010) 2477–2483.
[11] W.A. Khan, A. Aziz, Natural convection flow of a nanofluid over a vertical plate with uniform surface heat flux, Int. J. Therm. Sci. 50 (2011) 1207–1214.
[12] S. Ahmad, A.M. Rohni, I. Pop, Blasius and Sakiadis problems in nanofluids, Acta Mech. 218 (2011) 195–204.
[13] A.M. Rohni, S. Ahmad, I. Pop, Boundary layer flow over a moving surface in a nanofluid beneath a uniform free stream, Int. J. Heat Fluid Flow 21 (2011) 828–846.
[14] N. Bachok, A. Ishak, I. Pop, Flow and heat transfer over a rotating porous disk in a nanofluid, Phys. B 406 (2011) 1767–1772.
[15] N. Bachok, A. Ishak, I. Pop, Flow and heat transfer characteristics on a moving plate in a nanofluid, Int. J. Heat Mass Transfer 55 (2012) 642–648.
[16] A.M. Rohni, S. Ahmad, I. Pop, Flow and heat transfer over an unsteady shrinking sheet with suction in nanofluids, Int. J. Heat Mass Transfer 55 (2012) 1888–1895.
[17] K. Das, N. Acharya, P.K. Kundu, The onset of nanofluid flow past a convectively heated shrinking sheet in presence of heat source/sink: a Lie group approach, Appl. Therm. Eng. 103 (2016) 38–46.
[18] Y. Wang, J.M. Wu, Numerical simulation on single bubble behavior during Al2O3/H2O nanofluids flow boiling using Moving Particle Simi-implicit method, Prog. Nucl. Energy 85 (2015) 130–139.
[19] R. Turcu, A. Darabont, A. Nan, N. Aldea, D. Macovei, D. Bica, L. Vekas, O. Pana, M.L. Soran, A.A. Koos, L.P. Biro, New polypyrrole-multiwall carbon nanotubes hybrid materials, J. Optoelectron. Adv. M. 8 (2006) 643–647.
[20] S. Jana, A. Salehi-Khojin, W.H. Zhong, Enhancement of fluid thermal conductivity by the addition of single and hybrid nano-additives, Thermochim. Acta 462 (2007) 45–55.
[21] S. Suresh, K.P. Venkitaraj, P. Selvakumar, M. Chandrasekar, Effect of Al_2O_3−Cu/water hybrid nanofluid in heat transfer, Exp. Therm. Fluid Sci. 38 (2012) 54–60.
[22] M. Baghbanzadeha, A. Rashidib, D. Rashtchiana, R. Lotfib, A. Amrollahib, Synthesis of spherical silica/multi wall carbon nanotubes hybrid nano structures and investigation of thermal conductivity of related nanofluids, Thermochim. Acta 549 (2012) 87–94.
[23] O. Soltani, M. Akbari, Effects of temperature and particles concentrationon the dynamic viscosity of MgO-MWCNT/ethylene glycol hybrid nanofluid: Experimental study, Physica E 84 (2016) 564–570.
[24] M. Vafaei, M. Afrand, N. Sina, R. Kalbasi, F. Sourani, H. Teimouri, Evaluation of thermal conductivity of MgO-MWCNTs/EG hybrid nanofluids based on experimental data by selecting optimal artificial neural networks, Physica E 85 (2017) 90–96.
[25] T.H. Yen, C.Y. Soong, P.Y. Tzeng, Hybrid molecular dynamics-continuum simulation for nano/mesoscale channel flows, Microfluid Nanofluid 3 (6) (2007), 729 729.
[26] M.N. Labib, M.J. Nine, H. Afrianto, H. Chung, H. Jeong, Numerical investigation on effect of base fluids and hybridnanofluid in forced convective heat transfer, Int. J. Therm. Sci. 71 (2013) 163–171.
[27] R. Nasrin, M.A. Alim, Finite element simulation of forced convection in a flat plate solar collector: Influence of nanofluid with double nanoparticles, J. Appl. Fluid Mech. 7 (2014) 543–556.
[28] B. Takabi, H. Shokouhmand, Effects of Al_2O_3-Cu/water hybrid nanofluid on heat transfer and flow characteristics in turbulent regime, Int. J. Mod. Phys. C 26 (4) (2015) 1550047.
[29] S.S.U. Devi, S.P.A. Devi, Numerical investigation of three-dimensional hybrid Cu-Al_2O_3/water nanofluid flow over a stretching sheet with effecting Lorentz force subject to Newtonian heating, Can. J. Phys. 94 (2016) 490–496.
[30] S.S.U. Devi, S.P.A. Devi, Heat transfer enhancement of Cu-Al_2O_3/water hybrid nanofluid flow over a stretching sheet, J. Nigerian Mathem. Soc. 36 (2017) 419–433.
[31] R.M. Yousefi, S. Dinarvand, M.E. Yazdi, I. Pop, Stagnation-point flow of an aqueous titania-copper hybrid nanofluid toward a wavy cylinder, Int. J. Numer. Method Heat Fluid Flow 28 (2018) 1716–1735.
[32] T. Hayat, S. Nadeem, A.U. Khan, Rotating flow of Ag-CuO/H_2O hybrid nanofluid with radiation and partial slip boundary effects, Eur. Phys. J. E. 41 (2018) 75.
[33] S.S. Ghadikolaei, M. Yassari, H. Sadeghi, K. Hosseinzadeh, D.D. Ganji, Investigation on thermophysical properties of Tio2–Cu/H2O hybrid nanofluid transport dependent on shape factor in MHD stagnation point flow, Powder Technol. 322 (2017) 428–438.
[34] T. Tayebi, A.J. Chamkha, Buoyancy-driven heat transfer enhancement in a sinusoidally heated enclosure utilizing hybrid nanofluid, Comput. Therm. Sci.: Int. J. 9 (2017) 405–421.
[35] H.R. Ashorynejad, A. Shahriari, MHD natural convection of hybrid nanofluid in an open wavy cavity, Results. Phys. 9 (2018) 440–455.
[36] M. Ghalambaz, M.A. Sheremet, S.A.M. Mehryan, F.M. Kashkooli, I. Pop, Local thermal non-equilibrium analysis of conjugate free convection within a porous enclosure occupied with Ag–MgO hybrid nanofluid, J. Therm. Anal. Calorim. 1–18 (2018).
[37] H. Li, C.S. Ha, I. Kim, Fabrication of carbon nanotube/SiO2 and carbon nanotube/SiO2/Ag nanoparticles hybrids by using plasma treatment, Nanoscale Res. Lett. 4 (2009) 1384–1388.
[38] G. Paul, J. Philip, B. Raj, P.K. Das, I. Manna, Synthesis, characterization, and thermal property measurement of nano-$Al_{95}Zn_{05}$ dispersed nanofluid prepared by a two-step process, Int. J. Heat Mass Transfer 54 (2011) 3783–3788.
[39] S.K. Das, S.U.S. Choi, W. Yu, T. Pradeep, Nanofluids: Science and Technology, Wiley-Interscience, New Jersey, 2007.
[40] V. Trisaksri, S. Wongwises, Critical review of heat transfer characteristics of nanofluids, Renew. Sustain. Energy Rev. 11 (2007) 512–523.
[41] X.Q. Wang, A.S. Mujumdar, Heat transfer characteristics of nanofluids: A review, Int. J. Therm. Sci. 46 (2007) 1–19.
[42] X.Q. Wang, A.S. Mujumdar, A review on nanofluids – Part I: Theoretical and numerical investigations, Brazilian J. Chem. Eng. 25 (2008) 613–630.
[43] X.Q. Wang, A.S. Mujumdar, A review on nanofluids – Part II: Experiments and applications, Brazilian J. Chem. Eng. 25 (2008) 631–648.
[44] S. Kakac, A. Pramuanjaroenkij, Review of convective heat transfer enhancement with nanofluids, Int. J. Heat Mass Transfer 52 (2009) 3187–3196.
[45] A. Kamyar, R. Saidur, M. Hasanuzzaman, Application of computational fluid dynamics (CFD) for nanofluids, Int. J. Heat Mass Transfer 55 (2012) 4104–4115.
[46] J. Sarkar, P. Ghosh, A. Adil, A review on hybrid nanofluids: Recent research, development and applications, Renew. Sust. Energy Rev. 43 (2015) 164–177.
[47] S. Akilu, K.V. Sharma, A.T. Baheta, R. Mamat, A review of thermophysical properties of water based composite nanofluids, Renew. Sust. Energy Rev. 66 (2016) 654–678.
[48] J.R. Babu, K.K. Kumar, S.S. Rao, State-of-art review on hybrid nanofluids, Renew. Sust. Energy Rev. 77 (2017) 551–565.
[49] K.Y. Leong, K.Z. Ku Ahmad, H.C. Ong, M.J. Ghazali, A. Baharum, Synthesis and thermal conductivity characteristic of hybrid nanofluids – A review, Renew. Sust. Energy Rev. 75 (2017) 868–878.
[50] M.H. Ahmadi, A. Mirlohi, M.A. Nazari, R. Ghasempour, A review of thermal conductivity of various nanofluids, J. Mol. Liq. 265 (2018) 181–188.
[51] N. Ali, J.A. Teixeira, A. Addali, A review on nanofluids: Fabrication, stability, and thermophysical properties, J. Nanomater. 6978130 (2018).
[52] G. Huminic, A. Huminic, Hybrid nanofluids for heat transfer applications – A state-of-the-art review, Int. J. Heat Mass Transfer 125 (2018) 82–103.
[53] N.A.C. Sidik, I.M. Adamu, M.M. Jamil, G.H.R. Kefayati, R. Mamat, G. Najafi, Recent progress on hybrid nanofluids in heat transfer applications: A comprehensive review, Int. Commun. Heat Mass 78 (2016) 68–79.
[54] L.S. Sundar, K.V. Sharma, M.K. Singh, A.C.M. Sousa, Hybrid nanofluids preparation, thermal properties, heat transfer and friction factor – A review, Renew. Sust. Energy Rev. 68 (2017) 185–198.
[55] B.C. Sakiadis, Boundary-layer behaviour on continuous solid surfaces: I. Boundary layer equations for two-dimensional and axisymmetric flow, Am. Inst. Chem. Engineers J. 7 (1961) 26–28.
[56] L.J. Crane, Flow past a stretching plate, Z. Angew. Math. Phys. 21 (1970) 645–647.
[57] C.K. Chen, M.I. Char, Heat transfer of a continuous, stretching surface with suction or blowing, J. Math. Anal. Appl. 135 (1988) 568–580.
[58] C.Y. Wang, Free convection on a vertical stretching surface, J. Appl. Math. Mech. (ZAMM) 69 (1989) 418–420.
[59] H.I. Andersson, B.S. Dandapat, Flow of a power-law fluid over a stretching sheet, Stability Appl. Anal. Continuous Media 1 (1991) 339–347.
[60] R.S.R. Gorla, I. Sidawi, Free convection on a vertical stretching surface with suction and blowing, Appl. Sci. Res. 52 (1994) 247–257.
[61] C.H. Chen, Laminar mixed convection adjacent to vertical, continuously stretching sheets, Heat Mass Transfer 33 (1998) 471–476.
[62] E. Magyari, B. Keller, Exact solutions for self-similar boundary-layer flows induced by permeable stretching walls, Eur. J. Mech. B Fluids 19 (2000) 109–122.

[63] H.I. Andersson, Slip flow past a stretching surface, Acta Mech. 158 (2002) 121–125.
[64] A. Ishak, R. Nazar, I. Pop, Unsteady mixed convection boundary layer flow due to a stretching vertical surface, Arabian J. Sci. Eng. 31 (2006) 165–182.
[65] A. Ishak, R. Nazar, I. Pop, Boundary layer flow and heat transfer over an unsteady stretching vertical surface, Meccanica 44 (2009) 369–375.
[66] S. Goldstein, On backward boundary layers and flow in converging passage, J. Fluid Mech. 21 (1965) 33–45.
[67] C.Y. Wang, Liquid film on an unsteady stretching sheet, Q. Appl. Math. 48 (1990) 601–610.
[68] M. Miklavcic, C.Y. Wang, Viscous flow due to a shrinking sheet, Q. Appl. Math. 64 (2006) 283–290.
[69] T. Fang, W. Liang, C.F. Lee, A new solution branch for the Blasius equation – A shrinking sheet problem, Comput. Math. Appl. 56 (2008) 3088–3095.
[70] Fang, T.G.; Zhang, J.; SS Yao, J., Viscous flow over an unteady shrinking sheet with mass transfer, Chin. Phys. Lett. 26 (29), 2009, 014703.
[71] T. Fang, Boundary layer flow over a shrinking sheet with power-law velocity, Int. J. Heat Mass Transfer 51 (2008) 5838–5843.
[72] T. Fang, J. Zhang, Thermal boundary layers over a shrinking sheet: An analytical solution, Acta Mech. 209 (2010) 325–343.
[73] T. Hayat, Z. Abbas, M. Sajid, On the analytic solution of magnetohydrodynamic flow of a second grade fluid over a shrinking sheet, ASME J. Appl. Mech. 74 (2007) 1165–1171.
[74] M. Sajid, T. Hayat, T. Javed, MHD rotating flow of a viscous fluid over a shrinking surface, Nonlinear Dyn. 51 (2008) 259–265.
[75] C.Y. Wang, Stagnation flow towards a shrinking sheet, Int. J. Non Linear Mech. 43 (2008) 377–382.
[76] J.H. Merkin, V. Kumaran, The unsteady MHD boundary-layer flow on a shrinking sheet, Eur. J. Mech. B Fluids 29 (2010) 357–363.
[77] K. Bhattacharyya, Boundary layer flow and heat transfer over an exponentially shrinking sheet, Chin. Phys. Lett. 28 (7) (2011) 074701.
[78] K. Bhattacharyya, Effects of radiation and heat source/sink on unsteady MHD boundary layer flow and heat transfer over a shrinking sheet with suction/injection, Front. Chem. Sci. Eng. 5 (3) (2011) 376–384.
[79] N.A. Yacob, A. Ishak, Micropolar fluid flow over a shrinking sheet, Meccanica 47 (2012) 293–299.
[80] I.S. Awaludin, P.D. Weidman, A. Ishak, Stability analysis of stagnation-point flow over a stretching/shrinking sheet, AIP Adv. 6 (2016) 045308.
[81] S.K. Soid, A. Ishak, I. Pop, Unsteady MHD flow and heat transfer over a shrinking sheet with ohmic heating, Chin. J. Phys. 55 (4) (2017) 1626–1636.
[82] I. Pop, K. Naganthran, R. Nazar, A. Ishak, The effect of vertical throughflow on the boundary layer flow of a nanofluid past a stretching/shrinking sheet: A revised model, Int. J. Numer. Method H 27 (9) (2017) 1910–1927.
[83] K. Khanafer, K. Vafai, M. Lightstone, Buoyancy-driven heat transfer enhancement in a two-dimensional enclosure utilizing nanofluids, Int. J. Heat Mass Transfer 46 (2003) 3639–3653.
[84] H.F. Oztop, E. Abu-Nada, Numerical study of natural convection in partially heated rectangular enclosures filled with nanofluids, Int. J. Heat Fluid Flow 29 (2008) 1326–1336.
[85] J.H. Merkin, Mixed convection boundary layer flow on a vertical surface in a saturated porous medium, J. Eng. Math. 14 (1980) 301–313.
[86] P.D. Weidman, D.G. Kubitschek, A.M.J. Davis, The effect of transpiration on self-similar boundary layer flow over moving surfaces, Int. J. Eng. Sci. 44 (2006) 730–737.
[87] N.C. Roşca, I. Pop, Mixed convection stagnation point flow past a vertical flat plate with a second order slip: Heat flux case, Int. J. Heat Mass Transfer 65 (2013) 102–109.
[88] A.V. Roşca, I. Pop, Flow and heat transfer over a vertical permeable stretching/shrinking sheet with a second order slip, Int. J. Heat Mass Transfer 60 (2013) 355–364.
[89] S.D. Harris, D.B. Ingham, I. Pop, Mixed convection boundary-layer flow near the stagnation point on a vertical surface in a porous medium: Brinkman model with slip, Transp. Porous Media 77 (2009) 267–285.
[90] L.F. Shampine, I. Gladwell, S. Thompson, Solving ODEs with MATLAB, Cambridge University Press, Cambridge, 2003.